Supporting Information

For

Engineering Synergistic Di-Iron Sites and Anion Microenvironments in a Metal-Organic Framework Catalyst for Aerobic Wacker-Type Olefin Oxidation

Jun-Yu Li,[ab] Fu-Qi Mi [c] and Teng Zhang *[b]

[a] Fujian Science & Technology Innovation Laboratory for Optoelectronic Information of China, Fuzhou 350108, China.
[b] State Key Laboratory of Structural Chemistry, Fujian Institute of Research on the Structure of Matter, Chinese Academy of Sciences, Fuzhou 350002, China.
[c] Shandong Institute of Nonmetallic Materials, Jinan, Shandong 250031, China.
*Corresponding author: zhangteng@fjirsm.ac.cn

Contents

1. General Information

All chemicals were obtained from commercial sources (Adamas, Macklin, Energy Chemical, Strem, Sinopharm, etc.) and used without further purification. ^{1}H NMR data were collected on a Bruker AVANCE III HD (400 MHz) spectrometer. Chemical shifts were quoted in parts per million (ppm) referenced to the incomplete deuterated solvent peak (7.26 ppm for $CDCl_3$, 2.50 ppm for DMSO-d_6 or 3.31 ppm for CD_3OD) or TMS (0 ppm). Powder X-ray diffraction data (PXRD) were recorded on a Bruker-D8 Advance using Cu Kα radiation source (λ = 1.5418 Å). Infrared spectra were obtained in the 400−4000 cm^{-1} range using a Bruker VERTEX 70 spectrometer. Inductively coupled plasma optical emission spectrometry (ICP-OES) was performed on HORIBA Jobin Yvon-Ultima2. X-ray photoelectron spectroscopy (XPS) spectra were collected using a Thermo Fisher-ESCALAB 250Xi spectrometer. GC-MS measurements were conducted on a Shimadzu GCMS-QP2020 instrument. Nitrogen adsorption-desorption isotherms were collected on a Micromeritics ASAP 2460 Adsorption Analyzer at 77 K. UV-vis spectra were collected on a lampo 950 UV-vis spectrophotometer. Thermogravimetric analysis (TGA) was performed on a SDT Q600 with a heating rate of 5 °C/min under nitrogen flow (30 mL/min). Scanning electron microscopic (SEM) images were collected by a Hitachi SU-8010 microscope.

2. Characterization of MOF Materials and MOF-Fe Catalysts

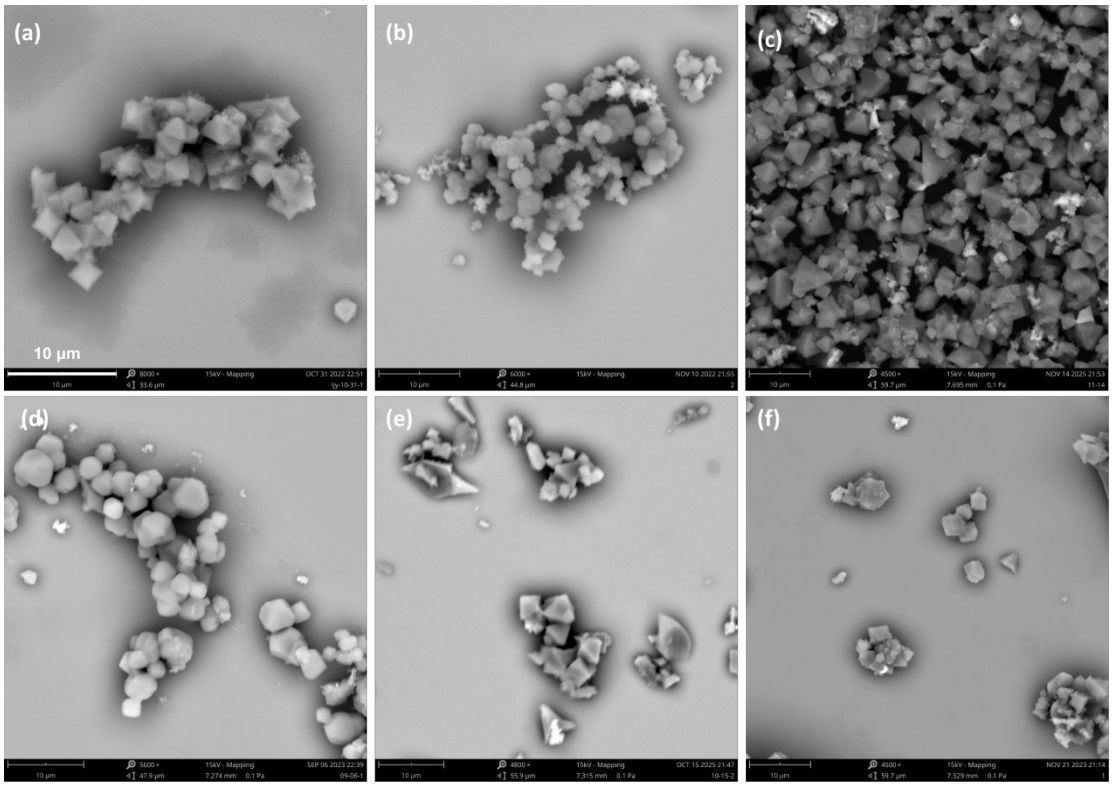

Figure S1. SEM images of (a) UiO-67-pyma, (b) UiO-67-pyma-d, (c) UiO-67-pyma-$FeCl_2$, (d) UiO-67-pyma-d-$FeCl_2$, (e) UiO-67-pyma-$Fe(OAc)_2$, (f) UiO-67-pyma-$FeCl_3$.

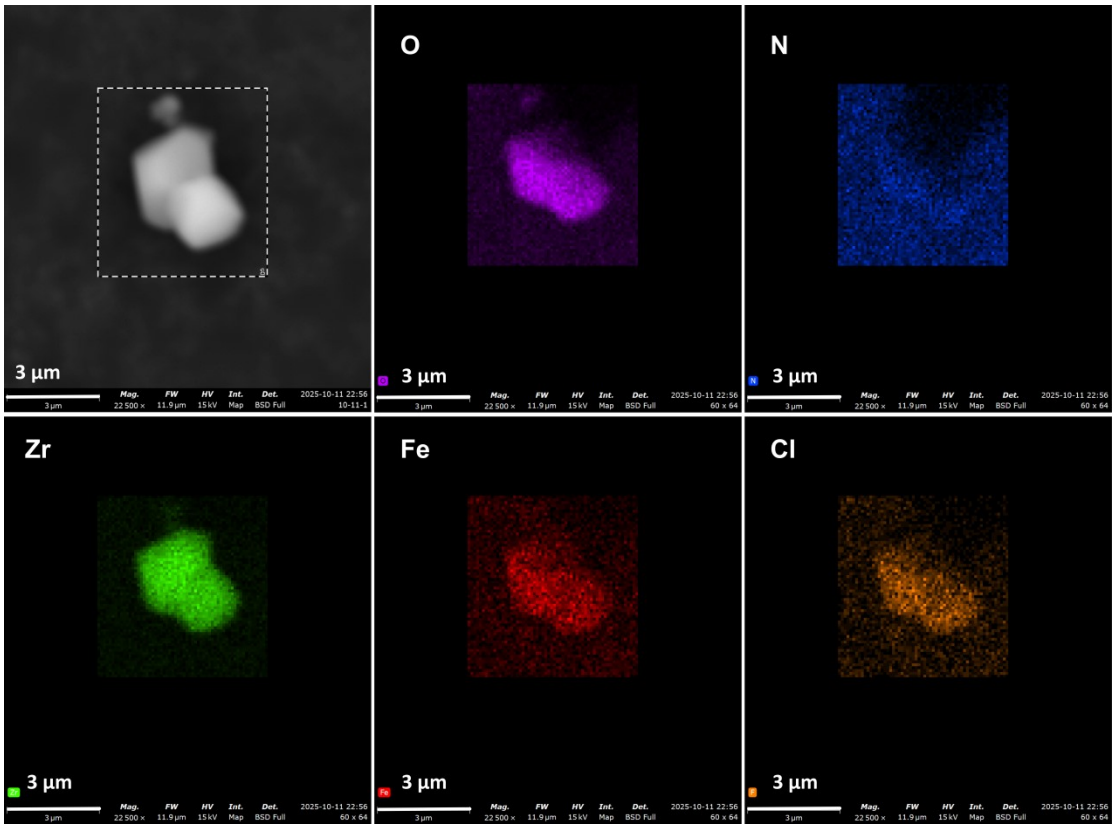

Figure S2. Energy-dispersive X-ray spectroscopy (EDS) elemental mapping of UiO-67-pyma-d-$FeCl_2$.

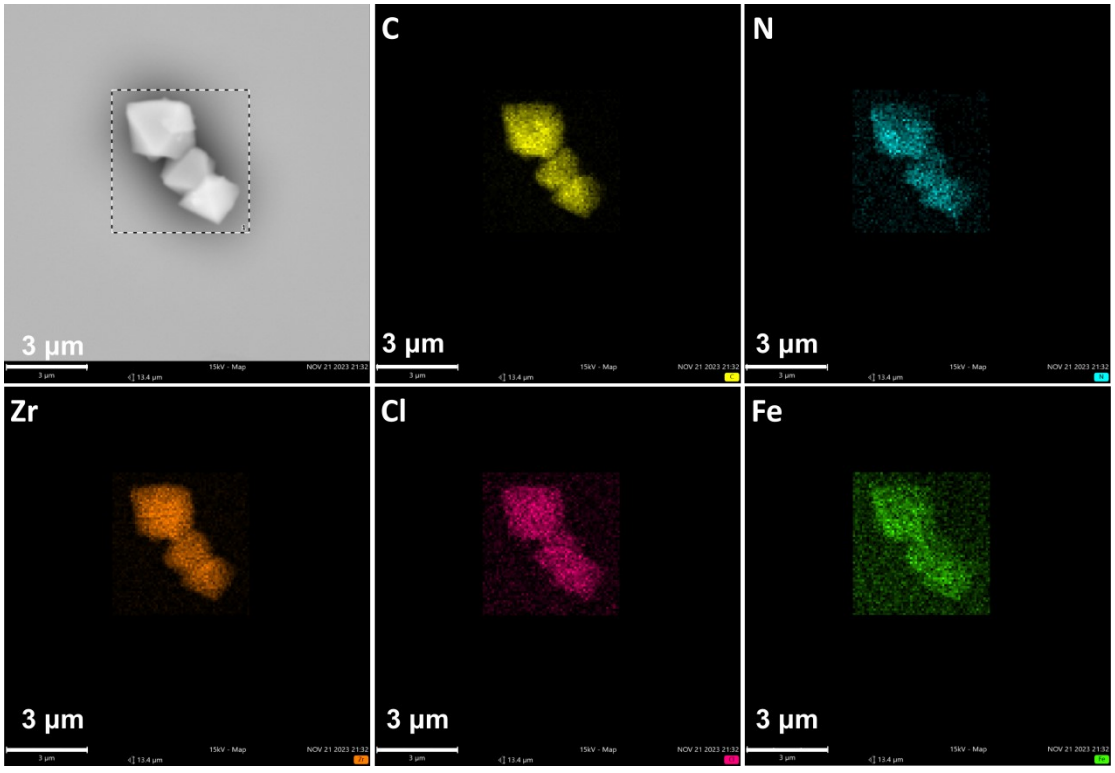

Figure S3. Energy-dispersive X-ray spectroscopy (EDS) elemental mapping of UiO-67-pyma-$FeCl_3$.

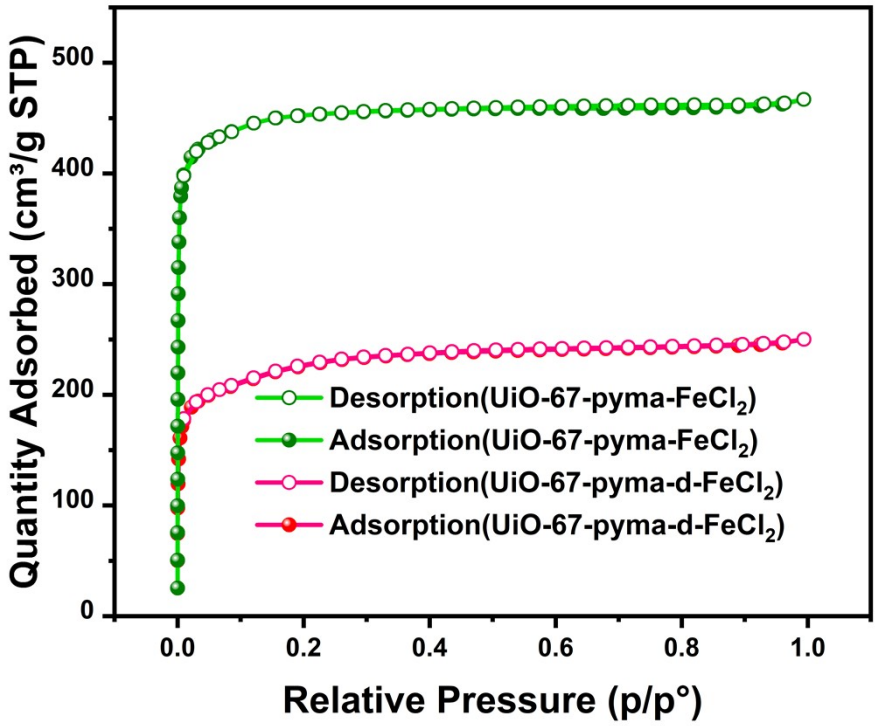

Figure S4. Nitrogen adsorption isotherms of UiO-67-pyma-$FeCl_2$ and UiO-67-pyma-d-$FeCl_2$.

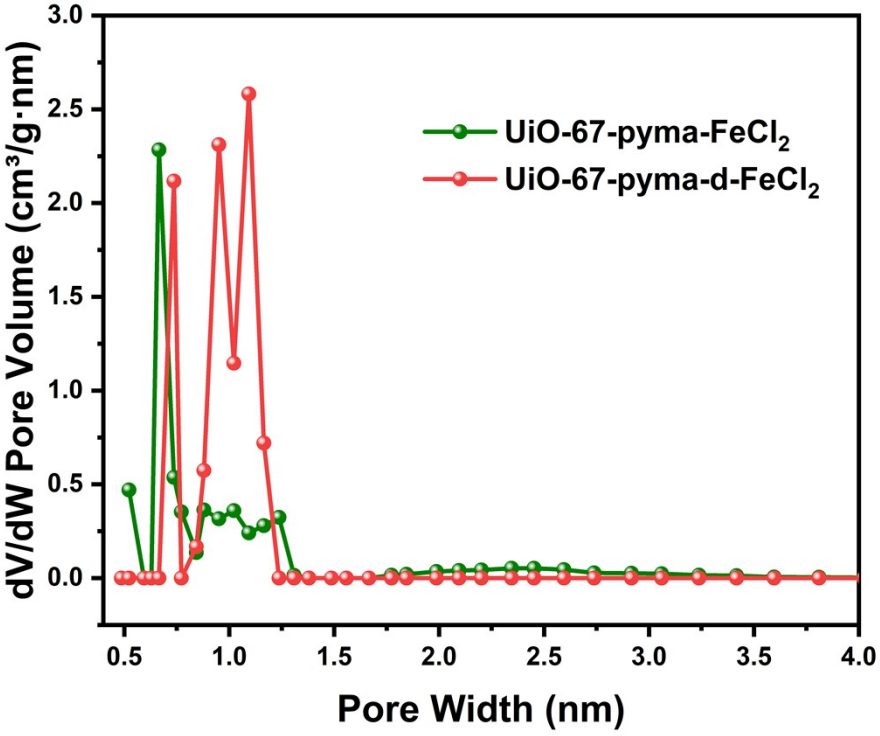

Figure S5. NL-DFT pore size distributions of UiO-67-pyma-$FeCl_2$ and UiO-67-pyma-d-$FeCl_2$.

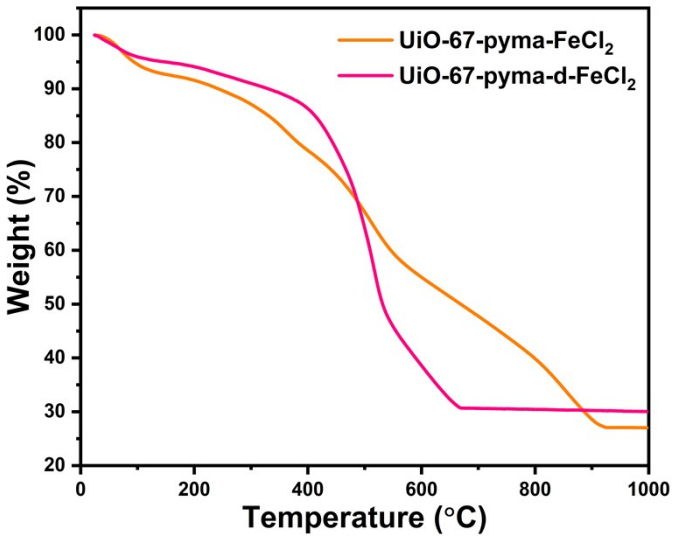

Figure S6. TGA trace of UiO-67-pyma-$FeCl_2$ and UiO-67-pyma-d-$FeCl_2$.

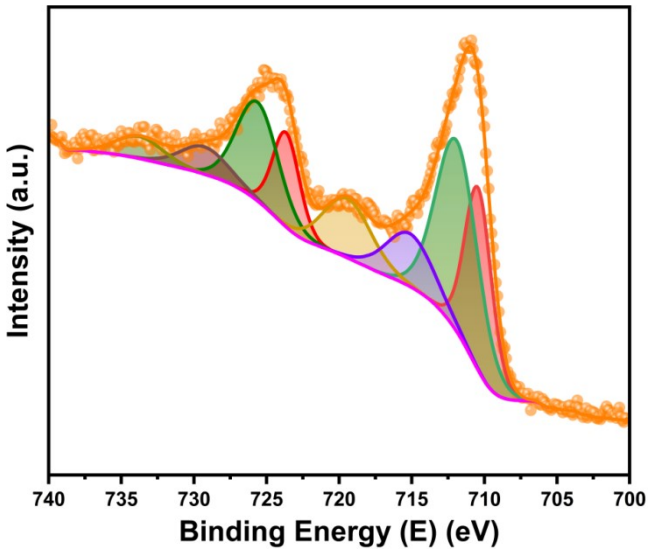

Figure S7. XPS spectra of Fe 3p for UiO-67-pyma-$FeCl_2$ after treatment with O_2 in ethanol.

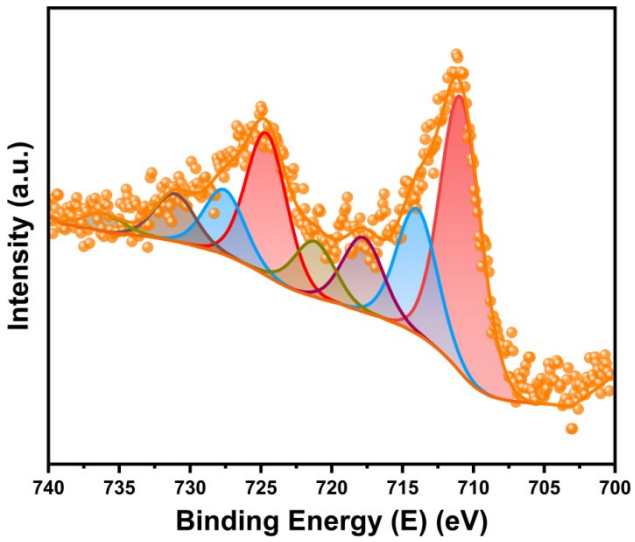

Figure S8. XPS spectra of Fe 3p for UiO-67-pyma-d-$FeCl_2$ after oxygen exposure.

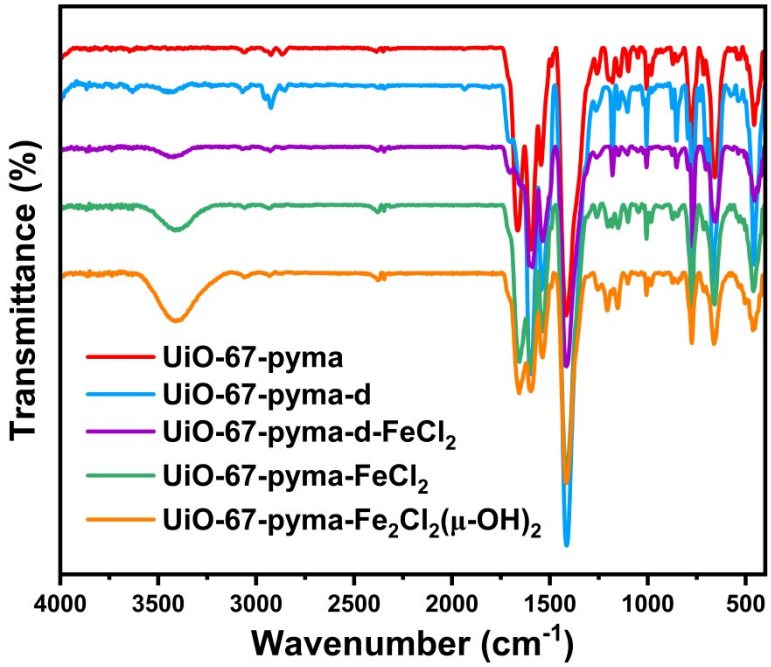

Figure S9. Full IR spectra of UiO-67-pyma, UiO-67-pyma-d, UiO-67-pyma-$FeCl_2$, UiO-67-pyma-d-$FeCl_2$ and UiO-67-pyma-$Fe_2(\mu\text{-}OH)_2$.

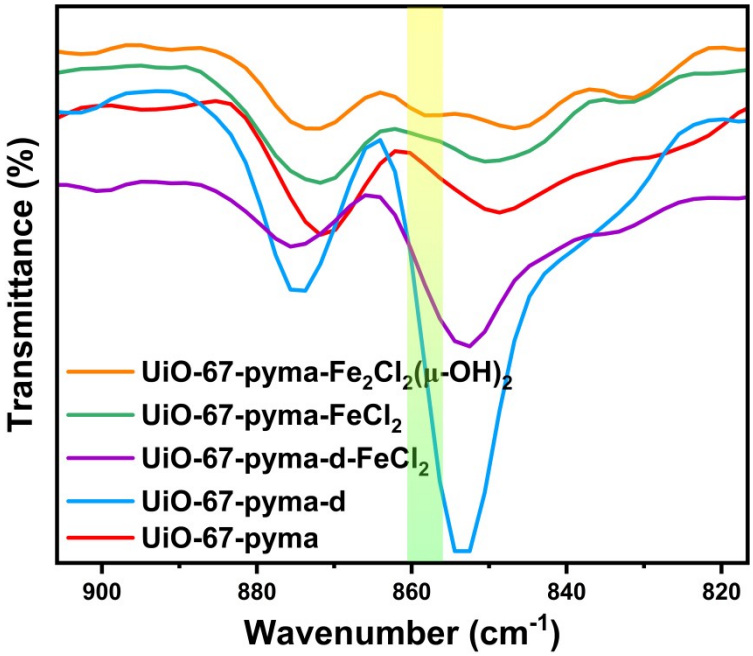

Figure S10. Characteristic IR signal of the $[Fe_2(\mu\text{-}OH)_2]_2$ moiety.

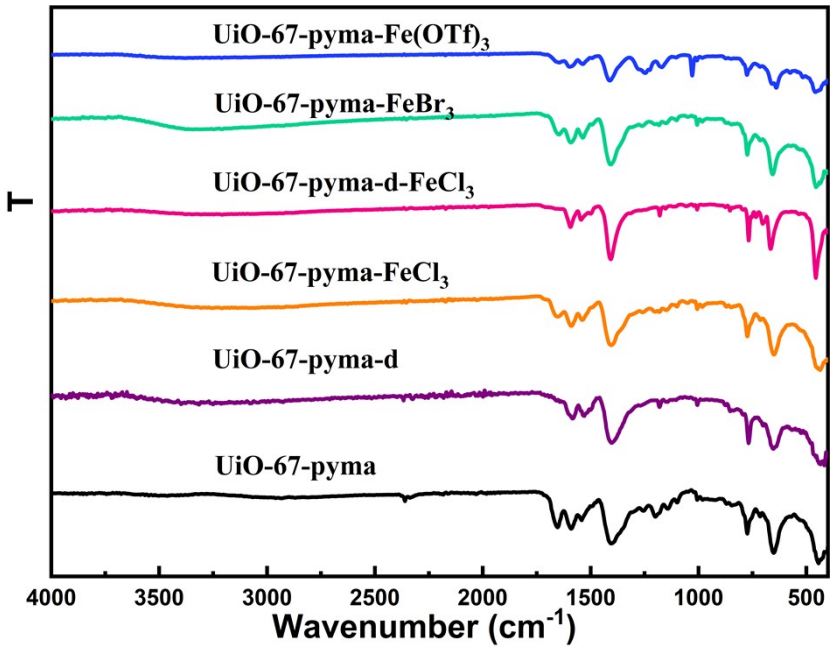

Figure S11. Infrared spectra of UiO-67-pyma, UiO-67-pyma-d, UiO-67-pyma-$FeCl_3$ and UiO-67-pyma-d-$FeCl_3$, UiO-67-pyma-$FeBr_3$ and UiO-67-pyma-$Fe(OTf)_3$.

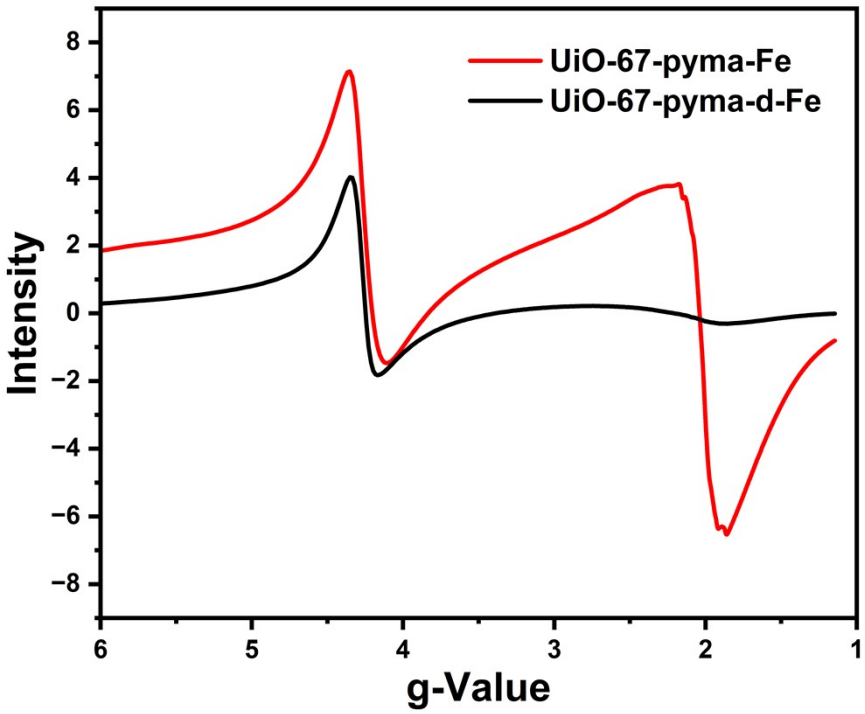

Figure S12. EPR spectra of oxidized UiO-67-pyma-$FeCl_2$ and UiO-67-yma-d-$FeCl_2$ measured at 100 K.

3. XAS Data Collection and Analysis

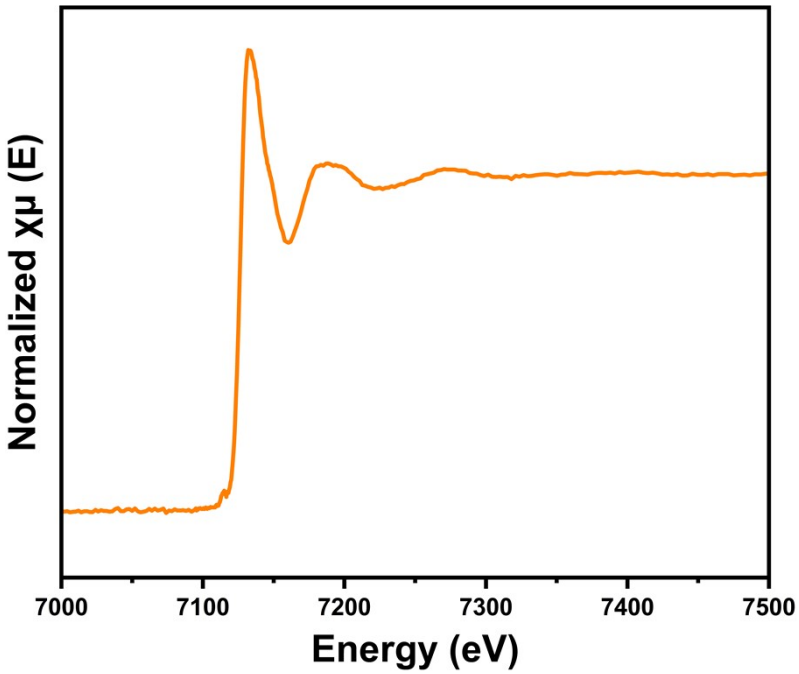

Figure S13. XAS spectrum of oxidized UiO-67-pyma-$FeCl_2$.

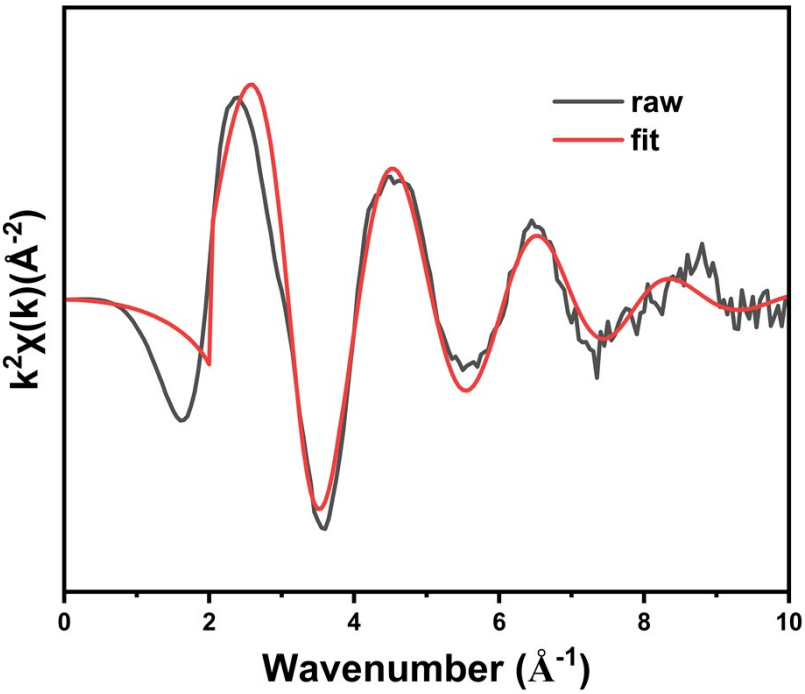

Figure S14. k-space EXAFS spectrum and fit of oxidized UiO-67-pyma-$FeCl_2$.

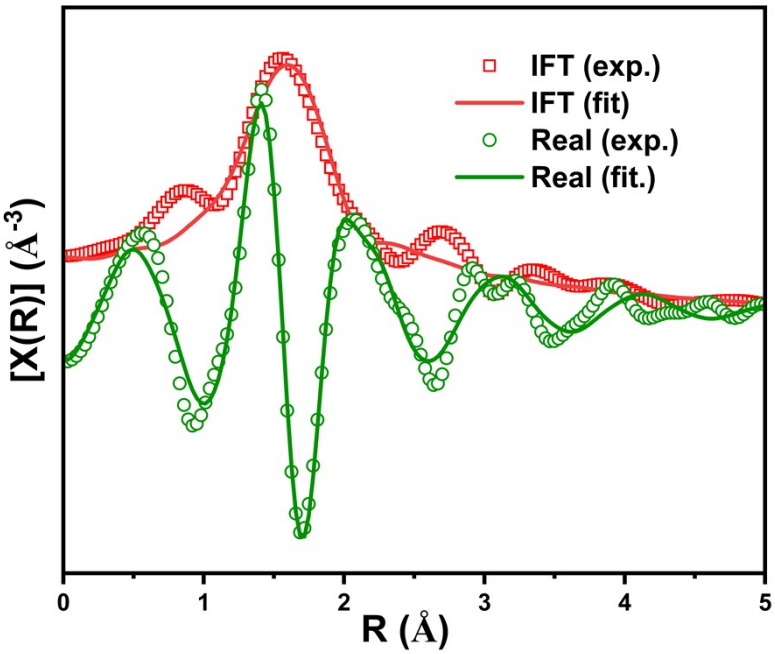

Figure S15. EXAFS spectra and fits in R-space at the Fe K-edge of oxidized UiO-67-pyma-$FeCl_2$ with the magnitude (open squares, red) and real components (open circles, green) of the Fourier transforms (FT).

Table S1. Summary of EXAFS fitting parameters for oxidized UiO-67-pyma-$FeCl_2$.

S_0^2	ΔE_0 (eV)	Path	N	R (Å)	$\sigma^2(10^{-3}$ Å$^2)$
1.58±0.72	15.95±2.41	Fe-N/O	5	2.02±0.03	14.1±4.8
		Fe-Cl	1	2.68±0.09	19.7±15.2

Fitting range: k 3-10 Å^{-1}, R 1.0-3.0 Å; Independent points: 8.6; Number of variables: 6; R-factor: 1.9%; Reduced chi-square:66.76.

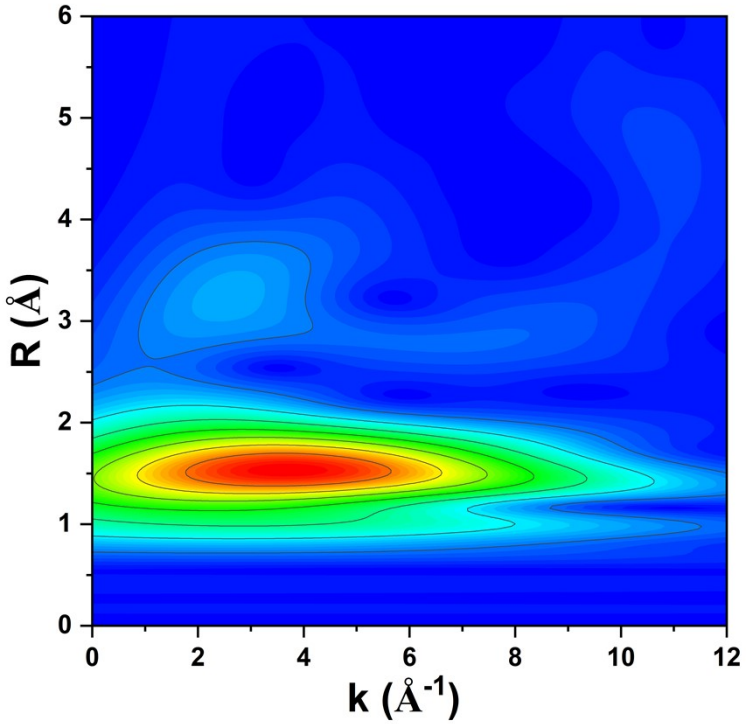

Figure S16. k^2-weighted wavelet transform for the Fe K-edge EXAFS spectrum of UiO-67-pyma-Fe.

4. Catalytic Wacker Type Olefin Oxidation

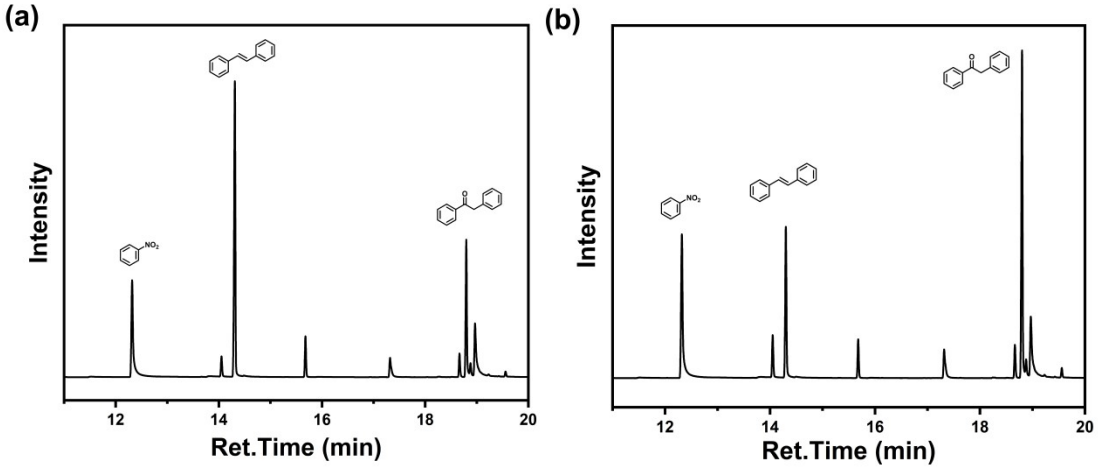

Figure S17. GC traces of the Wacker-type oxidation of trans-stilbene: (a) catalyzed by UiO-67-pyma-$FeCl_2$; (b) catalyzed by the homogeneous system $FeCl_2$/pymae (pymae= N-(2-pyridinylmethyl)ethylamine).

Table S2. Screening of hydride sources for the Wacker-type oxidation of olefins catalyzed by UiO-67-pyma-$FeCl_3$.

Entry[a]	Additive	Conversion/%	Yield (2a)/%	Yield (2b)/%
1	$PhSiH_3$	99.7	74	20
2	PMHS	8.0	6	2
3	DHP	0.9	0.07	0.5
5	Et_3SiH	5.1	0.2	1.5
6	Me_2PhSiH	4.3	0.5	1.6

7	TMDS	11.1	6.1	2.1
8	$(EtO)_3SiH$	29.5	12	5
9[b]	$(EtO)_3SiH$	99.5	61	20

[a] Reaction conditions: p-methoxystyrene (40 μL, 0.3 mmol), phenylsilane (74 μL,0.6 mmol), UiO-67-pyma-$FeCl_3$ (7.6 mg, 3 mol% for Fe), 2 mL EtOH, Stirred in the air. The conversions and yields were determined by GC. [b] The reaction time was extended to 72 h.

Table S3. Screening of temperature for Wacker oxidation reaction of olefins catalyzed by UiO-67-pyma-$FeCl_3$.

Entry	Temperature/ ℃	Time/h	Conversion/%	Yield(2a)/%	Yield(2b)/ %
1	10	120	100	77	13
2	25	12	99.7	74	20
3	50	12	99.8	51	43

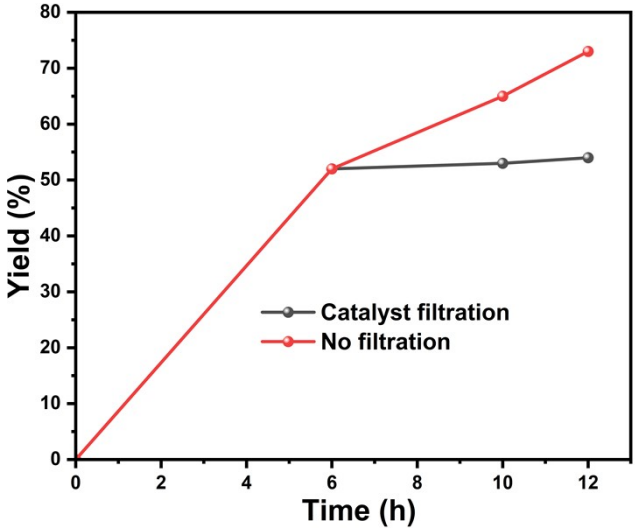

Figure S18. Hot filtration test for the Wacker-type oxidation of p-methoxystyrene catalyzed by UiO-67-pyma-$FeCl_2$ with 1 mol% Fe loading.

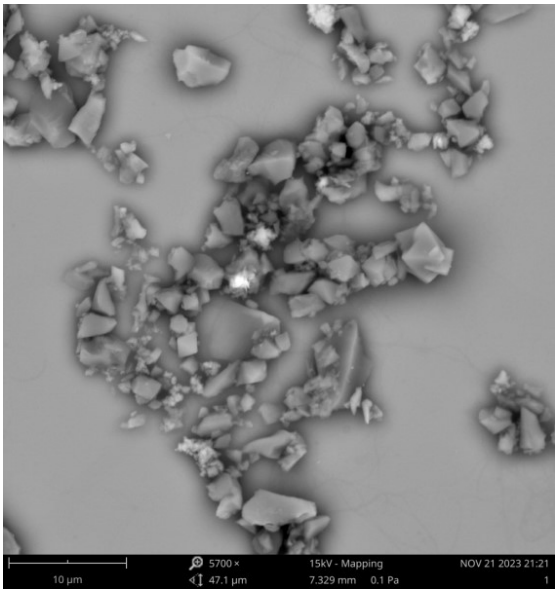

Figure S19. SEM image of the recovered catalyst after the catalytic reaction.

4.3 Gas chromatography testing

Table S5. Retention times of substrates and products in the catalytic reaction.

Substrate	Retention time	Product	Retention time
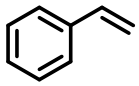	8.8 min	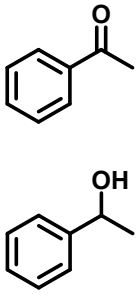	12.1 min 11.9 min
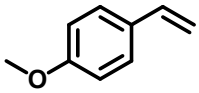	13.7 min	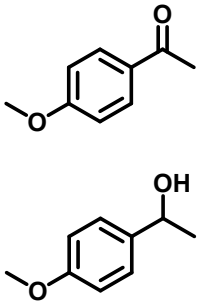	16.0 min 15.7 min
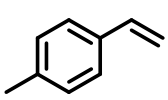	11.1 min	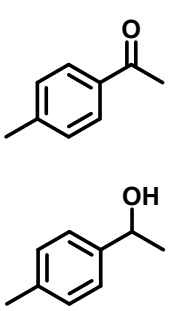	14.1 min 13.5 min

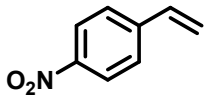	15.4 min	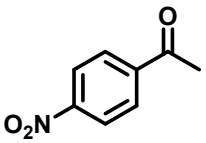 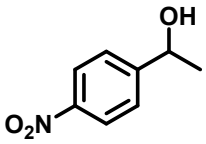	16.7 min 17.5 min
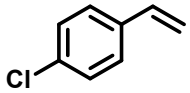	12.2 min	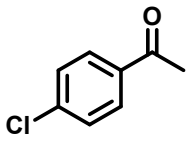 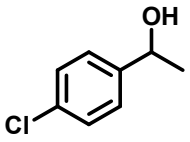	14.6 min 14.8 min
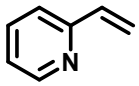	9.4 min	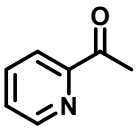	11.5 min
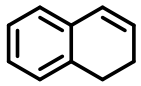	13.7 min	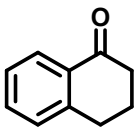 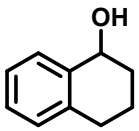	16.2 min 15.9 min
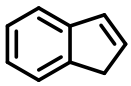	11.7 min	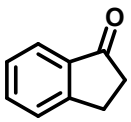	15.1 min
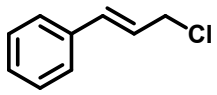	15.2 min	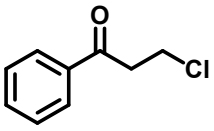	16.3 min

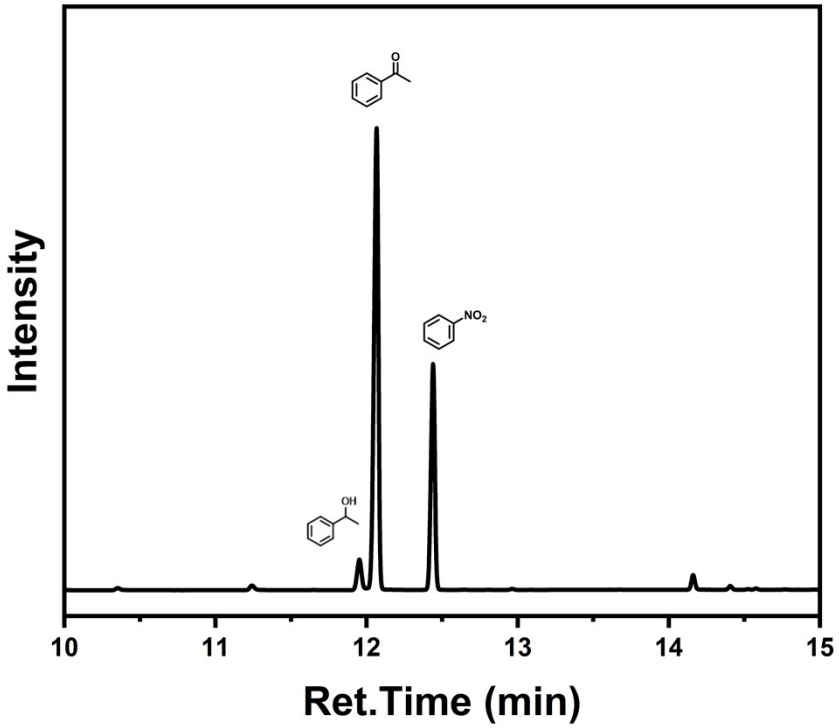
Intensity
10
11
12
13
14
15
Ret.Time (min)
O
NO2
OH

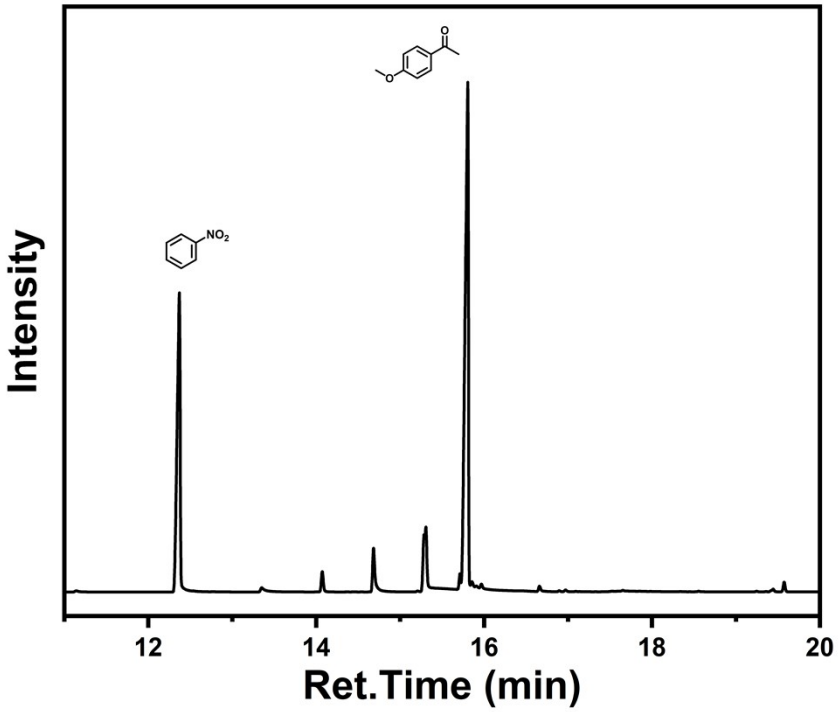
Intensity
12
14
16
18
20
Ret.Time (min)
O
O
NO2

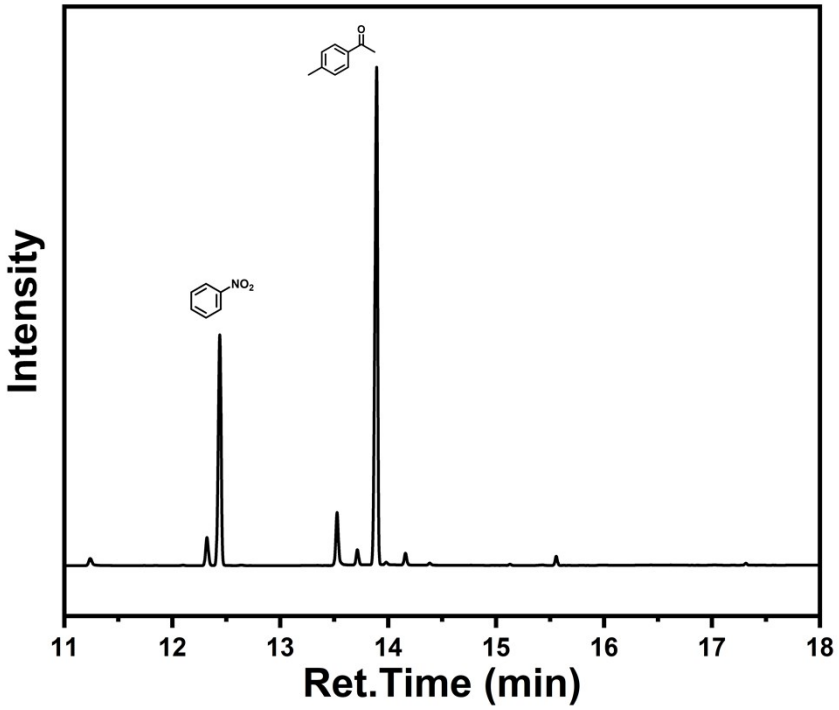
Intensity
11
12
13
14
15
16
17
18
Ret.Time (min)

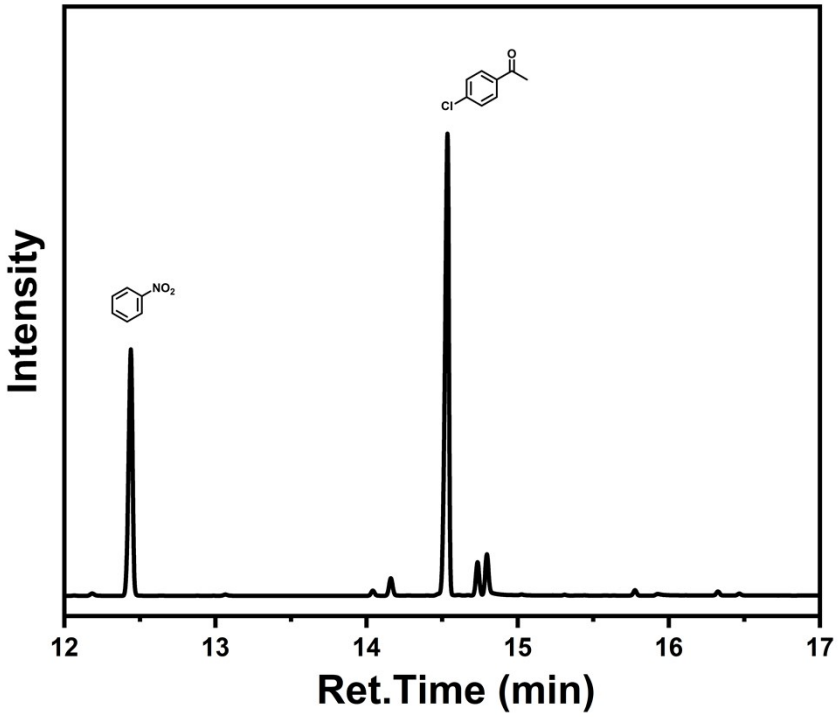
Intensity
12
13
14
15
16
17
Ret.Time (min)

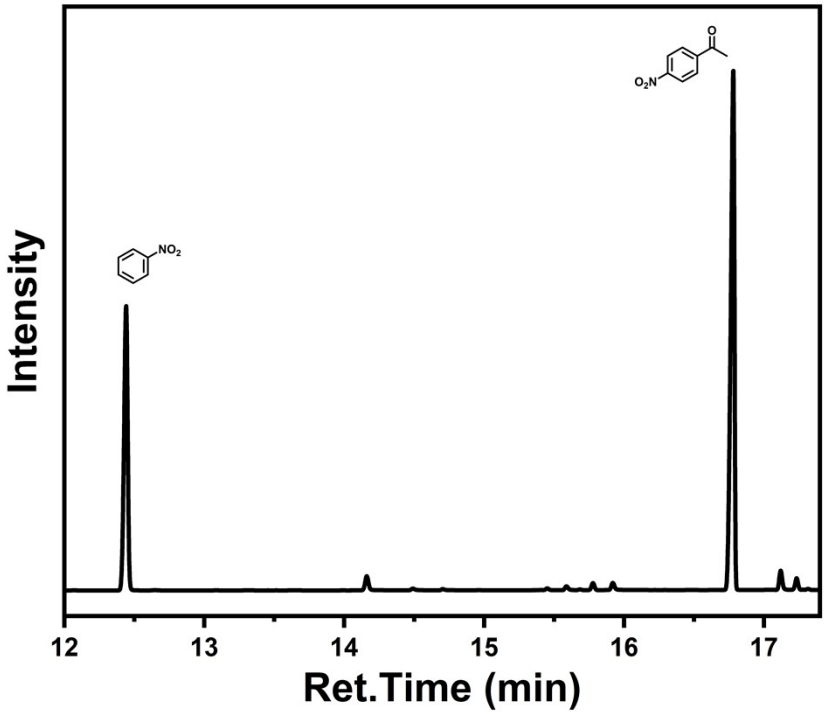
Intensity
12
13
14
15
16
17
Ret.Time (min)

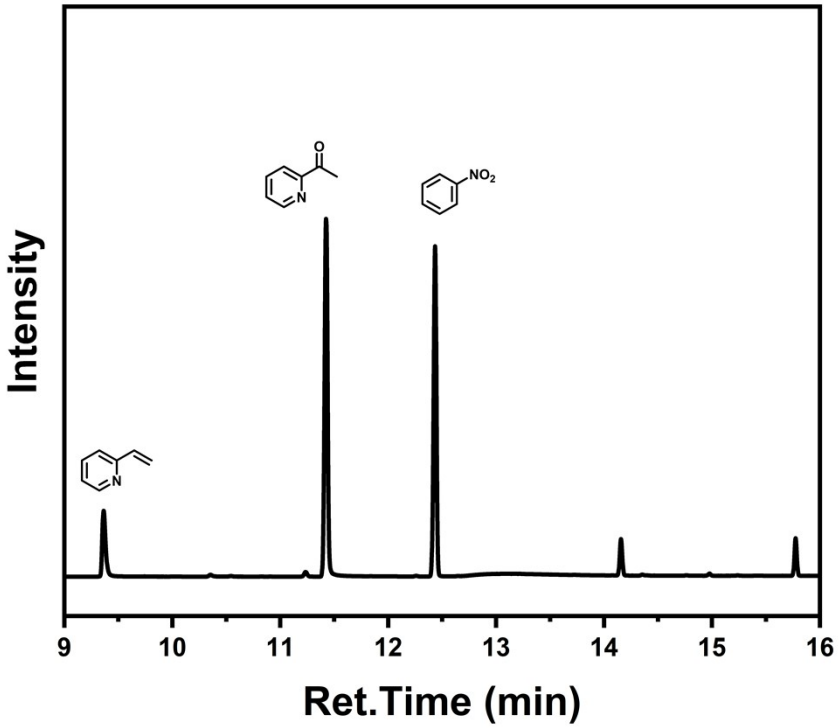
Intensity
9
10
11
12
13
14
15
16
Ret.Time (min)

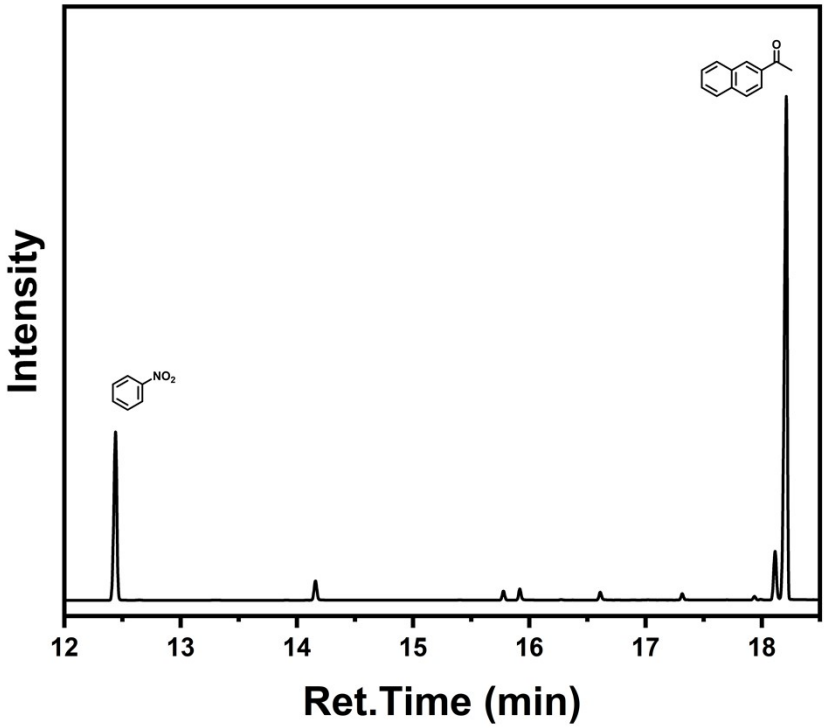
Intensity
NO2
O
12
13
14
15
16
17
18
Ret.Time (min)

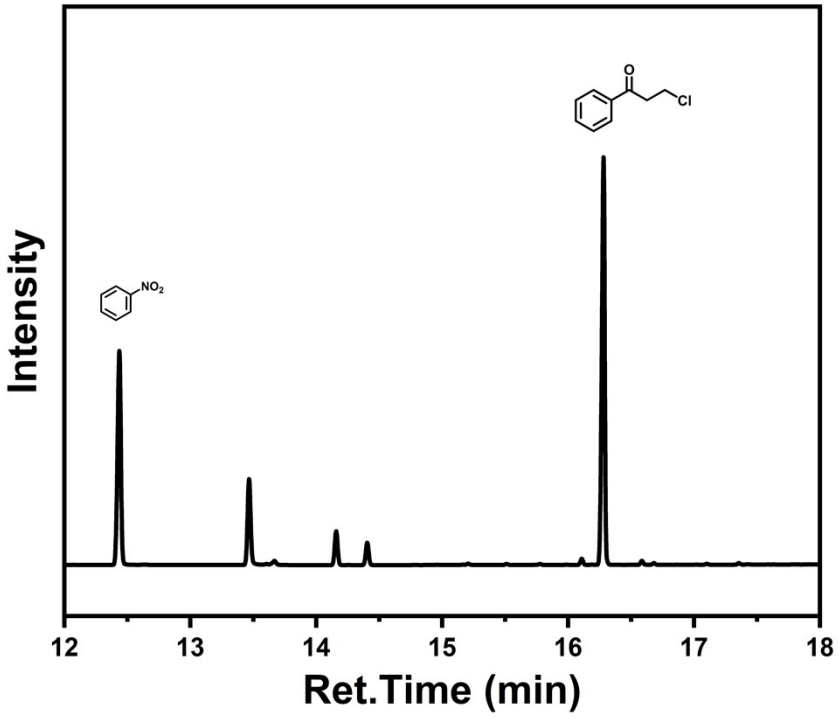
Intensity
NO2
O
Cl
12
13
14
15
16
17
18
Ret.Time (min)

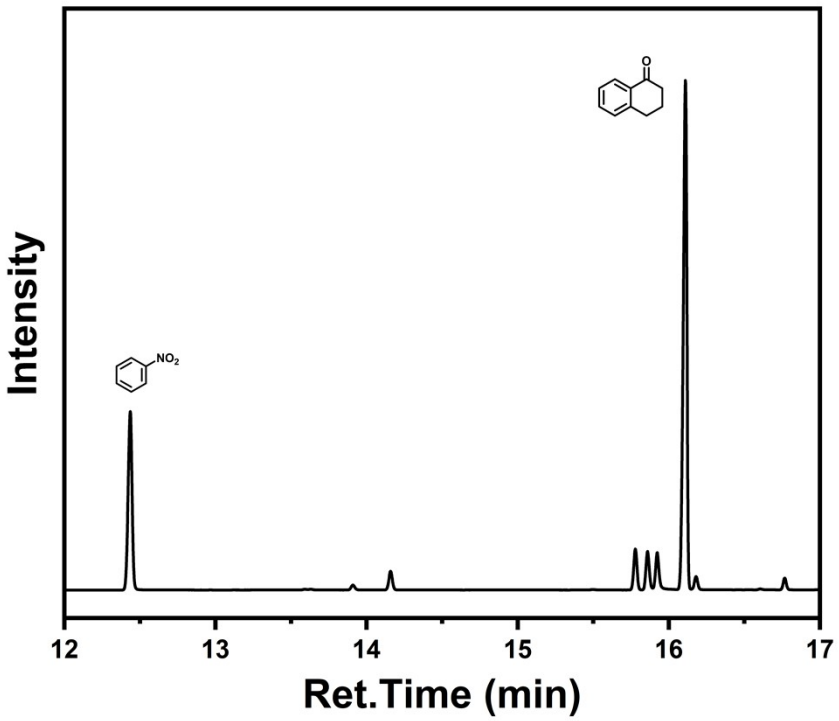

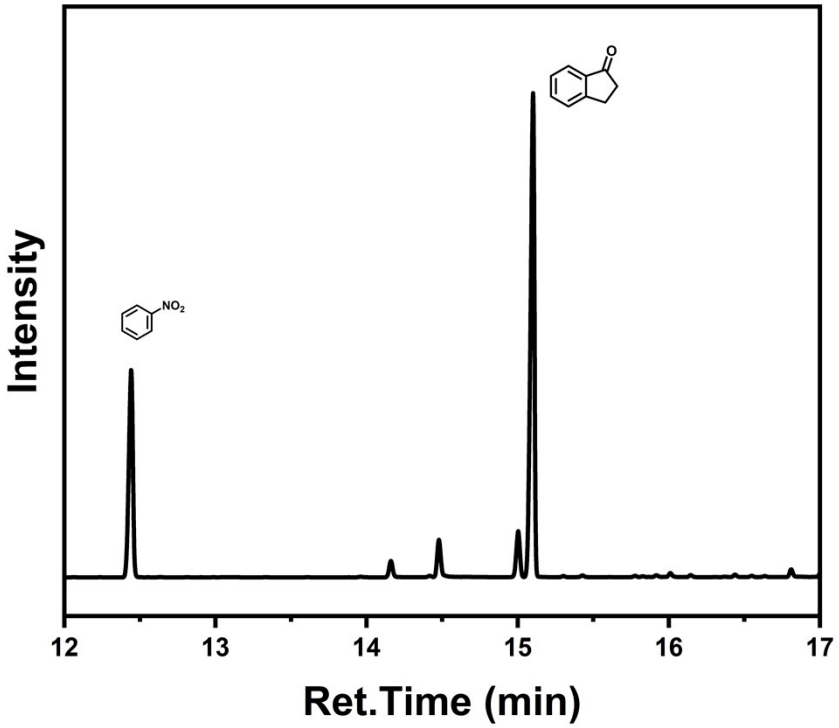

5. Catalytic activity comparison with previously reported catalysts.

Table S6. Comparison of Catalytic Activity in the Wacker-Type Oxidation of Styrene

over Various Fe- and Co-Based Catalysts.

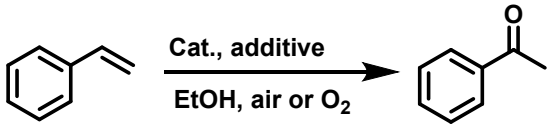

Entry	Catalyst	Reaction conditions	Yield/%	Ref.
1	$FeCl_2$ (10 mol%)	PMHS (3 equiv), EtOH, 80°C, and air.	84	[1]
2	$FePcF_{16}$ (5 mol%)	Et_3SiH (2 equiv), EtOH, r.t., O_2 (1 atm).	68	[2]
3	iron(III)-porphyrin complex Fe-1 (2.5 mol %)	$PhSiH_3$ (3 equiv), EtOH, r.t., air.	96	[3]
4	Fe/porphyrin (2.5 mol %)	$PhSiH_3$ (2 equiv), α-cyclodextrin (0.5 equiv), 15 μL of DMSO, 25 °C, air.	94	[4]
5	CoTPP (1 mol %)	PMHS (1 equiv), EtOH, 70°C, O_2 (1 bar)	81	[5]
6	SBA-15-A-S-Co (20 mg/mmol olefin)	$PhSiH_3$ (2 equiv), EtOH, 50°C, O_2 (1 atm).	80	[6]
7	UiO-67-pyma-$FeCl_2$ (3 mol %)	$PhSiH_3$ (1.2 equiv), EtOH, r.t., air.	94	This work

6. References

1. Liu, B.; Jin, F.; Wang, T.; Yuan, X.; Han, W., Wacker-Type Oxidation Using an Iron Catalyst and Ambient Air: Application to Late-Stage Oxidation of Complex Molecules. *Angew Chem Int Ed Engl* **2017,** *56* (41), 12712-12717.

2. Puls, F.; Knölker, H. J., Conversion of Olefins into Ketones by an Iron-Catalyzed Wacker-type Oxidation Using Oxygen as the Sole Oxidant. *ANGEWANDTE CHEMIE-INTERNATIONAL EDITION* **2018,** *57* (5), 1222-1226.

3. Trouvé, J.; Youssef, K.; Kasemthaveechok, S.; Gramage-Doria, R., Catalyst Complexity in a Highly Active and Selective Wacker-Type Markovnikov Oxidation of Olefins with a Bioinspired Iron Complex. *ACS Catalysis* **2023,** *13* (7), 4421-4432.

4. Jiang, C.; Wu, Y.; Zhang, Y.; Zong, J.; Wang, N.; Liu, G.; Liu, R.; Yu, H., Supramolecular Modulation for Selective Mechanochemical Iron-Catalyzed Olefin Oxidation. *Angewandte Chemie International Edition* **2025,** *64* (1), e202413901.

5. Abuhafez, N.; Gramage-Doria, R., Cobalt-Catalyzed Wacker-Type Aerobic Oxidation of Olefins into Ketones Enabled by PMHS: Giving Value to a Chemical Waste with Optimal Atom-Economy. *ChemCatChem* **2024,** *16* (16), e202400333.

6. Chang, C.; Hou, Y.; Li, J., Heterogeneous cobalt-complex catalyst for wacker-type oxidation of styrene by balloon O2. *Molecular Catalysis* **2025,** *577*, 114959.